Available online at www.sciencedirect.com
SCIENCE DIRECT
Journal of Chromatography B, 835 (2006) 62–70
JOURNAL OF CHROMATOGRAPHY B
www.elsevier.com/locate/chromb

Liquid chromatography electrospray ionization mass spectrometry analysis of the ocular metabolites from a short interfering RNA duplex

Michael Beverly *, Kim Hartsough, Lynn Machemer, Pam Pavco, Jennifer Lockridge

Sirna Therapeutics Inc., 2950 Wilderness Place, Boulder, CO 80301, USA

Received 15 November 2005; accepted 5 March 2006
Available online 30 March 2006

Abstract

The ocular metabolism of an siRNA duplex, SIRNA-027, was examined by ion-pair reversed-phase liquid chromatography (IP-RP-LC) coupled to electrospray ionization mass spectrometry (ESI–MS). The RNA duplex was injected intraocularly into the eyes of New Zealand white rabbits. Rabbits were sacrificed at different timepoints and the vitreous and retina/choroid tissue analyzed for siRNA by IP-RP-LC-MS. The method used a hexafluoroisopropanol (HFIP)/triethylamine (TEA) ion-pairing buffer with a methanol gradient. Using electrospray ionization, the duplex was preserved in the gas phase for analysis by a triple quadrupole mass spectrometer. With this methodology metabolites from rabbit ocular vitreous humor and retina/choroid tissue were identified and a pattern of siRNA degradation was established. Results showed that the duplex was metabolized predominantly from one end. This end of the siRNA duplex was calculated to have the weakest binding energy of the two ends indicating that the ability of the siRNA to split into single strands is a factor in its degradation.

Keywords: siRNA; HPLC; VEGF; Electrospray; RNAi; LC–MS; Metabolites; Oligonucleotides; Mass spectrometry; ESI

1. Introduction

The mechanism known as RNA interference (RNAi) has become one of the most important tools used in molecular biology. Protein synthesis in both plants and mammals can be significantly shutdown by the inhibitory RNA pathway [1,2]. The RNAi pathway utilizes short pieces (19–21 nucleotides) of double-strand RNA (called short interfering RNA or siRNA) that interact with a protein complex, termed the RNA induced silencing complex (RISC). The RISC machinery unwinds the duplex so that a single strand remains associated with the protein complex. Once part of the RISC complex, the single strand can act as a template to bind a complementary target strand of mRNA. Upon binding, the target mRNA strand is cleaved and is thereby prevented from being translated.

Due to the power of the RNAi pathway to prevent protein synthesis, short duplexes of RNA are being investigated as a possible treatment for a variety of indications including cancer, viral infection, and ocular disease [3–9]. As siRNA compounds are being explored as possible therapeutics, analytical methods that can study duplex RNA will be important in evaluating their pharmacokinetics and metabolism. Among the many methods used to study RNA, mass spectrometry with electrospray ionisation (ESI) has special advantages. Unlike chromatographic techniques where analyte identity is based on retention time, mass spectrometry analysis provides the molecular weight of the analyte, a property inherent to the analyte. This information has been used to determine exact nuclease cleavage sites in antisense metabolism studies and has helped to identify aspects of the siRNA mechanism [10–12]. The soft ionization process of ESI also allows duplex oligonucleotides to be mass analyzed intact and not denatured into single strands, a characteristic of the technique particularly applicable to siRNA analysis [13–22].

While there are many examples of ESI being used to examine RNA and DNA, most of the work has involved the direct infusion of samples and without on-line chromatographic separation. A major hindrance to the LC–MS analysis of oligonucleotides is the incompatibility between the common reversed-phase ion-pairing buffer system used to analyze oligonucleotides, triethylammonium acetate (TEAA), and electrospray ionization. To overcome this challenge other ion pairing buffers have been developed, most notably the HFIP/TEA system by

* Corresponding author. Tel.: +1 303 546 8190; fax: +1 303 449 8829.
E-mail address: beverlym@sirna.com (M. Beverly).

1570-0232/$ – see front matter © 2006 Elsevier B.V. All rights reserved.
doi:10.1016/j.jchromb.2006.03.008

Apffel et al. [23,24]. With the development of ESI compatible ion-pairing buffers, reversed-phase chromatography coupled with ESI has been used extensively to study oligonucleotides [10,11,25–29]. Even double strand DNA has been chromatographically separated and mass analyzed intact using this methodology [26,30,31]. Coupling reversed-phase chromatography to ESI provides other advantages such as allowing for high-throughput analysis and providing a way to desalt oligonucleotides. Cation adduction is a significant interferent in the ESI analysis of oligonucleotides and reversed-phase chromatography is one of a variety of methods used to reduce ubiquitous sodium adducts.

Preliminary work in our lab demonstrated the feasibility of using reversed-phase chromatography with ion-pairing reagents to analyze metabolites of duplex RNA [22]. We reported that duplex RNA could be electrosprayed and analyzed intact by using the HFIP/TEA ion-pairing buffer system. Here we expand on those initial findings and apply the method to an animal study using SIRNA-027, an siRNA duplex directed against vascular endothelial growth factor receptor 1 (VEGFR1). The VEGF receptor 1 has been implicated in the progression of age related macular degeneration (AMD) a disease affecting the retina that is the leading cause of blindness in the population over age 65 [32].

To study the stability of the siRNA duplex in the ocular tissues, SIRNA-027 was injected into the eyes of New Zealand white rabbits and samples were collected at various timepoints and analyzed by IP-RP-LCMS. Metabolite species were identified which provided insight into the degradation process and demonstrated the usefulness of the technique in siRNA studies.

2. Experimental

2.1. RNA oligonucleotides

The RNA duplex oligonucleotide SIRNA-027 was synthesized in-house using traditional phosphoramidite chemistry [33]. The sequence and molecular weights of the sense and antisense strands are (from 5′ to 3′) BCUGAGUUUAAAAGGCACCCTTB (7013.2 u) and GGGUGCCUUUUAAACUCAGT$_S$T (6663.0 u), respectively. The siRNA duplex has a molecular weight of 13676.3 u. The strands are composed of RNA bases with the uppercase T representing the DNA base thymine and the uppercase B representing an inverted abasic residue. Abasic groups were placed on the ends of the strands to prevent nuclease degradation [34]. In addition, the antisense oligonucleotide contains a phosphorothioate linkage between the two terminal thymines represented by the lower case s. The phosphorothioate linkage has been demonstrated to inhibit nuclease degradation and increase the lifetime of oligonucleotides [35,36]. Complementary strands were annealed in PBS, desalted and lyophilized.

The internal standard used in these experiments was a 30 nucleotide single strand RNA containing 2′-*O*-methyl nucleotides and four phosophorothioate linkages. The chemical modifications greatly increased the retention time and allowed the internal standard to elute after the siRNA duplex.

2.2. LC–MS

A Shimadzu HPLC system (Columbia, MD, USA) comprising two LC-10ADvp pumps, an SPD-10Avp UV–vis detector and a SCL-10Avp system controller were connected in-line to a Sciex API 365 triple quadrupole mass spectrometer (Applied Biosystems, Foster City, CA, USA). Samples were introduced via a Perkin-Elmer Series 200 auto sampler (Wellesley, MA, USA) and reversed-phase chromatography was carried out with an XTerra MSC18, 3.5 μm particle size, 2.1 mm × 150 mm column (Waters, Milford, MA, USA). Mobile phase buffer A consisted of 200 mM hexafluoroisopropanol (HFIP) and 8.15 mM triethylamine (TEA) in water at pH 7.9. Buffer B consisted of 200 mM HFIP and 8.15 mM TEA in 50% methanol/water. The flow rate was set to 120 μl/min.

For denaturing experiments the HPLC column was heated to 65 °C and the siRNA duplex was split into its two complementary strands. The gradient used for denaturing experiments was 30% buffer B ramped linearly over 5 min to 45% and then to 80% by 20 min. For chromatography of the intact duplex, the column was kept at 25 °C and buffer B was changed to 100% methanol. The gradient for duplex analysis was 20% B and ramping to 40% over 20 min. The HFIP, TEA, and methanol from Aldrich were used without further purification.

The eluent from the UV detector (set at 260 nm) on the HPLC was connected directly to the electrospray interface of the Sciex API 365 triple quadrupole MS via 127 μm ID PEEK tubing. A switching valve (Valco Inc., Houston, TX, USA) was placed in-line after the UV detector to direct early eluting salts to waste. To help control cation adduction, a small cation exchange guard column (Opti-Lynx, Optimize Technologies, Oregon City, OR, USA) was installed in-line directly before the MS.

The Sciex API 365 was operated in negative ionization mode for all analyses and the mass range of 800–1900 *m*/*z* was scanned with a 0.1 a.m.u. width step size over a 3 s scan time. The curtain gas was nitrogen and the source was kept at 200 °C. Electrospray ionization spectra were summed over a UV peak of interest and the multiple charge states were deconvoluted using the BioAnalyst software (Version 1.4) supplied by Applied Biosystems. The values presented in the resulting deconvoluted spectra are average masses since isotopic resolution was not achieved and the mass error of the system is 0.01%. Metabolites were identified by comparing the experimentally observed masses to a table of possible 3′ and 5′ nuclease derived metabolites.

2.3. Animal samples

SIRNA-027 (0.5 mg/eye) was injected intravitreally into female New Zealand white rabbits and animals were sacrificed at various time points. Vitreous humor was collected from the excised eye and isolated in a pre-weighed FastPrep (Q-biogene, Carlsbad, CA, USA) ceramic bead tube. When the cornea was cut away from the eye, the viscous portion of vitreous humor was then expressed and added to the rest of the vitreous sample. The entire sample was frozen on CO_2 (s) and kept at −80 °C until analysis. Retina/choroid samples were collected as one tissue from the scleral layers and placed in pre-weighed

FastPrep ceramic bead tubes. Prior to analysis, the vitreous and retina/choroid samples were homogenized and sample aliquots were taken.

2.4. Extraction of siRNA and metabolites

SIRNA-027 was extracted from vitreous samples by placing a volume of sample into Phase-lock "light" gel tubes (Eppendorf, Hamburg, Germany) containing 800 μL of 10 mM Tris/1 mM EDTA buffer. To this mixture, 100 μL of Phenol/Chloroform/isoamyl alcohol (25:24:1), 1 mM Tris/EDTA, pH 8.0 was added, and 100 μL of the internal standard at 10 μg/mL. The tubes were shaken and then centrifuged at 16,000 × *g* for 5 min. The aqueous layer was transferred to an eppendorf tube and then vacuum dried down in a SpeedVac (Savant Instruments Inc., Farmington, NY, USA) for 2.5 h. The dried sample was then resuspended in 100 μL of HPLC mobile phase A and 40 μL injected on column. The amount of vitreous sample used for extraction was chosen to provide samples that fell in the range of 100 μg/mL for early timepoints down to 10 μg/mL for later timepoints. An extraction volume of 10 μL was used for all time points except Days 4, 5, and 7, where 100 μL was used.

A modified procedure from the Mirvana RNA extraction kit (Ambion Inc., Austin, TX, USA) was used to extract SIRNA-027 from the retina/choroid samples. Retina–choroid samples (1 mg) were placed into a FastPrep ceramic bead tube with 0.5 mL of the Mirvana lysis buffer. After homogenization, 100 μL of the sample was added to an eppendorf tube along with 10 μL of Mirvana additive and 100 μL of water. To this mixture 100 μL of phenol:chloroform (5:1) isoamyl alcohol, pH 4.7 was added and the solution vortexed for 5 s. After mixing, the solution was centrifuged at 16,000 × *g* for 5 min. The top aqueous layer was transferred to a 1 mL eppendorf tube containing 800 μL of ethanol and was then mixed. This solution was transferred to a Mirvana glass fiber spin filter in two 400 μL aliquots. The glass fiber spin filter was spun at 16,000 × *g* for 15 s and the filtrate was discarded. The filter was washed twice by adding 400 μL of 80% ethanol and then spinning at 16,000 × *g* for 15 s and discarding the filtrate. After washing, the RNA was eluted from the glass fiber filter into a new eppendorf tube with 200 μL of water. The water sample was then dried down using a Speed-Vac on high for 2 h and then stored at −80 °C until needed. The samples were resuspended in 100 μL of mobile phase A prior to analysis. Three vitreous and three retina/choroid samples were available for each time point. To avoid possible carry over, the last time point samples were analyzed first as these had the least amount of siRNA.

To assess the efficiency of the phenol:chloroform extraction procedure, SIRNA-027 was spiked into vitreous fluid and the extracted samples were analyzed by the LC–MS method and UV 260 nm peak areas were recorded. Spiking SIRNA-027 into vitreous fluid showed an extraction recovery for the phenol:chloroform method that varied over the 10–100 μg/mL concentration range ($n = 4$/sample concentration). Recoveries of samples in vitreous ranged from 14% for 10 μg/mL samples up to 40% for 100 μg/mL samples compared to samples in water which gave greater than 90% recovery across the concentration range. The reproducibility of the vitreous extractions also varied over the concentration range with lower concentration samples having relative standard deviations (RSD) ranging between 30% for the 10 μg/mL concentrations down to 5% for 100 μg/mL samples compared to water extracts which had an RSD of 3% across the concentration range. The negative effect of the vitreous fluid on extraction recoveries and RSD prevented this procedure from being used in an absolute quantitative manner.

3. Results and discussion

3.1. Single strand analysis

In order to produce the most complete picture of siRNA metabolism, SIRNA-027 was analyzed both as an intact duplex and denatured into its complementary single strands. During these analyses it became clear that there were certain advantages to denaturing the duplex. Resolution of the column was improved at the higher temperatures needed to denature the duplex and there was inherently better resolution of the smaller oligonucleotides over the larger duplex. The ESI spectra were also improved when running at elevated column temperatures. Single strand oligonucleotides had less salt adducts and noise than the duplex, and the ion signal intensity of the single strands was greater than the duplex. Some signal increase has to do with the smaller size of the single strands compared to the duplex but the heat itself also appeared to increase the signal strength by possibly improving evaporation of the mobile phase.

Representative chromatograms of SIRNA-027 in vitreous fluid taken from selected timepoints are displayed in Fig. 1. The UV chromatograms (260 nm) of the samples show the increase in metabolites relative to the full-length strands over the time course of the experiment. By Day 7 there was little UV signal detected for the full-length strands or metabolites. A comparison of the chromatograms from the vitreous and the retina/choroid tissue revealed that the samples had the same pattern of metabolites (Fig. 2). Metabolite patterns at each time point were also very similar between the three animals examined (data not shown).

Early timepoint samples contained two major peaks in the UV chromatogram at 24.5 and 20.4 min which corresponded to the full-length sense and antisense strands, respectively. The representative ESI spectra for the two single strands are shown in Fig. 3. Under the LC–MS conditions used for this experiment, the single strand oligonucleotides had charge state envelopes centered around the −5 and −6 charge states. Deconvolution of the spectra yielded masses of 7013 and 6663 corresponding to the sense and antisense strands, respectively.

Metabolites were identified by deconvoluting the mass spectra for an LC peak and then comparing this mass to a table of possible 5′ and 3′ nuclease derived metabolites. In this paper a shorthand nomenclature will be used to describe metabolites. The sense or antisense strand will be designated S or AS, respectively, followed by the number of bases lost in parentheses with N being the full-length strand. The side of the strand from which the loss occurs follows as either 3′ or 5′. For example,

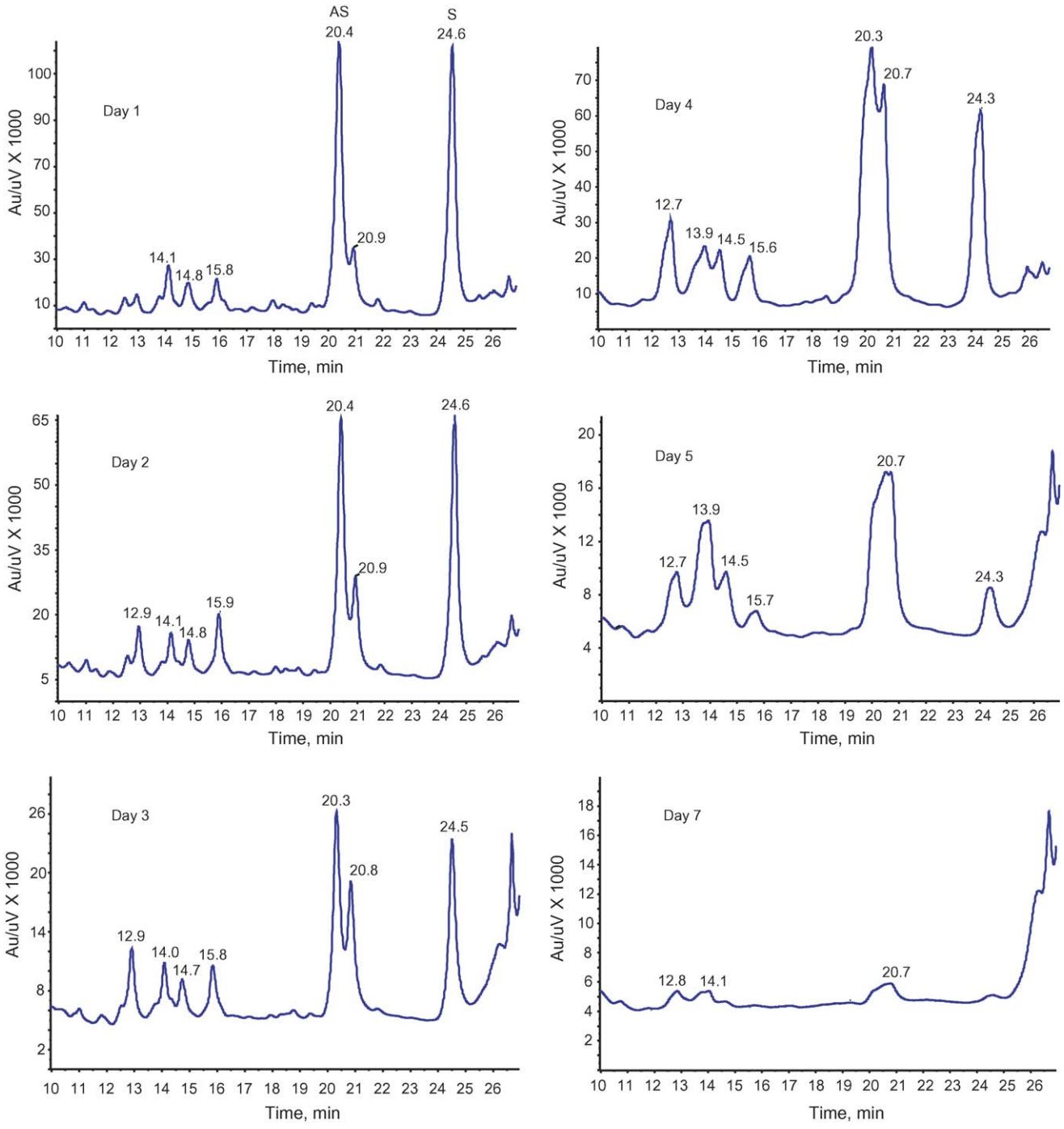

Fig. 1. UV 260 nm chromatograms of the vitreous extracts from various timepoints. Full-length sense and antisense strands are designated S and AS, respectively.

an examination of the mass spectra for the largest growing metabolite at 20.8 min identified that peak as belonging to the sense strand cleaved at the 3rd ribophosphate linkage from the 5′ end having a mass of 6222. This metabolite is designated S(N-3)5′. All of the identified metabolites are summarized in Table 1. Metabolites were consistent between the animals and the metabolite species in the vitreous humour were the same as those observed in the retina/choroid tissue. Agreement between vitreous and retina/choroid samples was expected as the UV chromatograms showed the same peaks.

The degradation species with the greatest relative peak area was the N-3 product from the 5′ end of the sense strand which eluted around 20.9 min. Endonuclease activity is hypothesized as the cause of this primary metabolite. The 5′ end of the sense strand is protected from exonuclease degradation by the abasic endgroup (no (N-1)5′ species was observed) but an endonuclease can skip inward to avoid this protection and cleave the strand. Once the protecting abasic group is gone degradation can proceed sequentially as is evidenced by the observed metabolites (Table 1). An unprotected version of SIRNA-027 degraded in

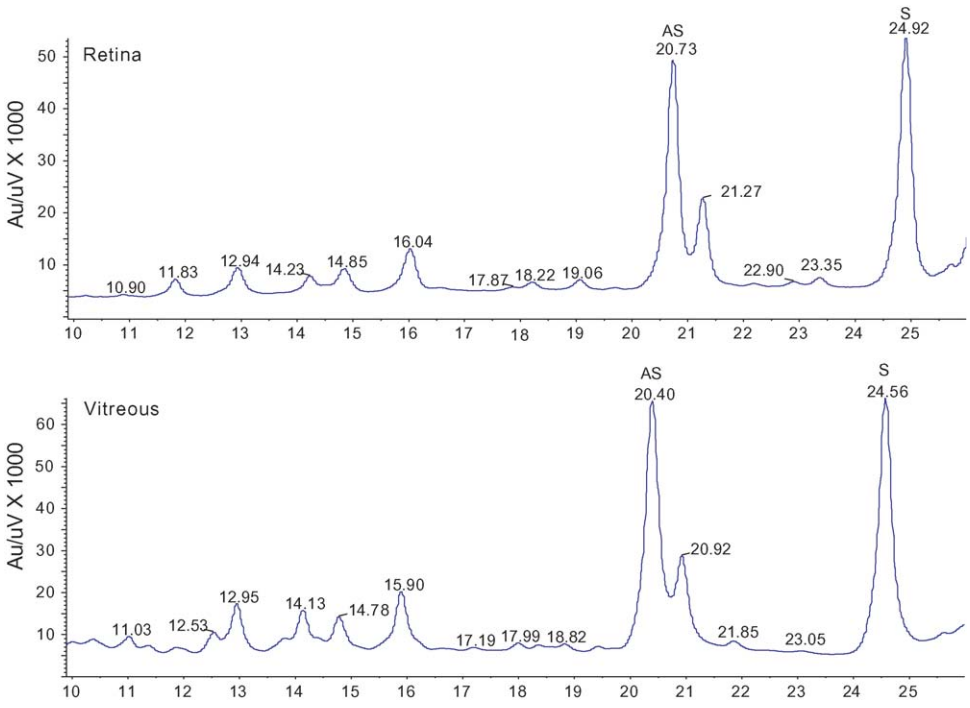

Fig. 2. The UV 260 nm chromatograms of vitreous and retina/choroid samples taken at the Day 3 time point.

a sequential fashion with (N-1)5′ species observed (results not shown).

The majority of the antisense degradation products were from nuclease attack on the phosphorothioate protected 3′ side of the strand. Unlike the sense strand, no one particular metabolite species was dominant. Due to the minimally observed (N-1)3′ metabolite species, it appeared that internal cleavage of the strand was also caused by a nuclease skipping inwards to avoid the terminal phosphorothioate linkage.

Interestingly, the least protected section of both the strands, the unmodified G's on the 5′ end of the antisense strand, showed little degradation. It is possible that the lack of degradation on this end of the antisense strand was due to its double strand character. This 5′ end of the antisense strand does not overhang its complementary pair but is bound to form a duplex. The double strand structure of this end could be imparting protection from nucleases as has been demonstrated for siRNAs in plasma [37].

In order to gain a better idea of the relative amounts of the metabolite versus the full-length strands, peak areas of the single strands and the major metabolite species were plotted as a ratio to the internal standard (Fig. 4). This plot displays a gradual growth of the major sense N-3 metabolite while the full-length sense and antisense strands decrease. All the species, including the metabolism products, show a gradual decrease in peak area

Table 1
Single strand species observed from the denaturing LC/MS analysis of vitreous samples

	Nucleotide loss	Peak assignment (min)	Observed mass	Theoretical mass
Sense Sequence				
5′-BCUGAGUUUAAAAGGCACCCTTB-3′	S	24.5	7013	7013.2
5′-UGAGUUUAAAAGGCACCCTTB-3′	S(N-2)5′	21.8	6528	6527.9
5′-GAGUUUAAAAGGCACCCTTB-3′	S(N-3)5′	20.9	6222	6221.7
5′-UUAAAAGGCACCCTTB-3′	S(N-7)5′	16.1	4897	4896.0
5′ UAAAAGGCACCCTTB-3′	S(N-8)5′	14.7	4589	4589.8
5′-AAAAGGCACCCTTB 3′	S(N-9)5′	14.1	4284	4283.6
5′-AAAGGCACCCTTB-3′	S(N-10)5′	12.5	3954	3954.4
5′-AAGGCACCCTTB-3′	S(N-11)5′	11.1	3625	3625.2
Antisense sequence				
5′-GGGUGCCUUUUAAACUCAGTsT-3′	AS	20.4	6663	6663.0
5′-GGGUGCCUUUUAAACUCAGT-3′	AS(N-1)3′	17.9	6342	6342.8
5′-GGGUGCCUUUUAAACUCAG-3′	AS(N-2)3′	15.9	6038	6038.5
5′-GGGUGCCUUUUAAACUCA-3′	AS(N-3)3′	14.7	5694	5693.3
5′-GGGUGCCUUUUAAACUC-3′	AS(N-4)3′	12.9	5365	5364.1
5′-CUUUUAAACUCAGTsT-3′	AS(N-6)5′	13.8	4671	4670.8
5′-UUUAAACUCAGTsT-3′	AS(N-8)5′	11.0	4060	4059.5

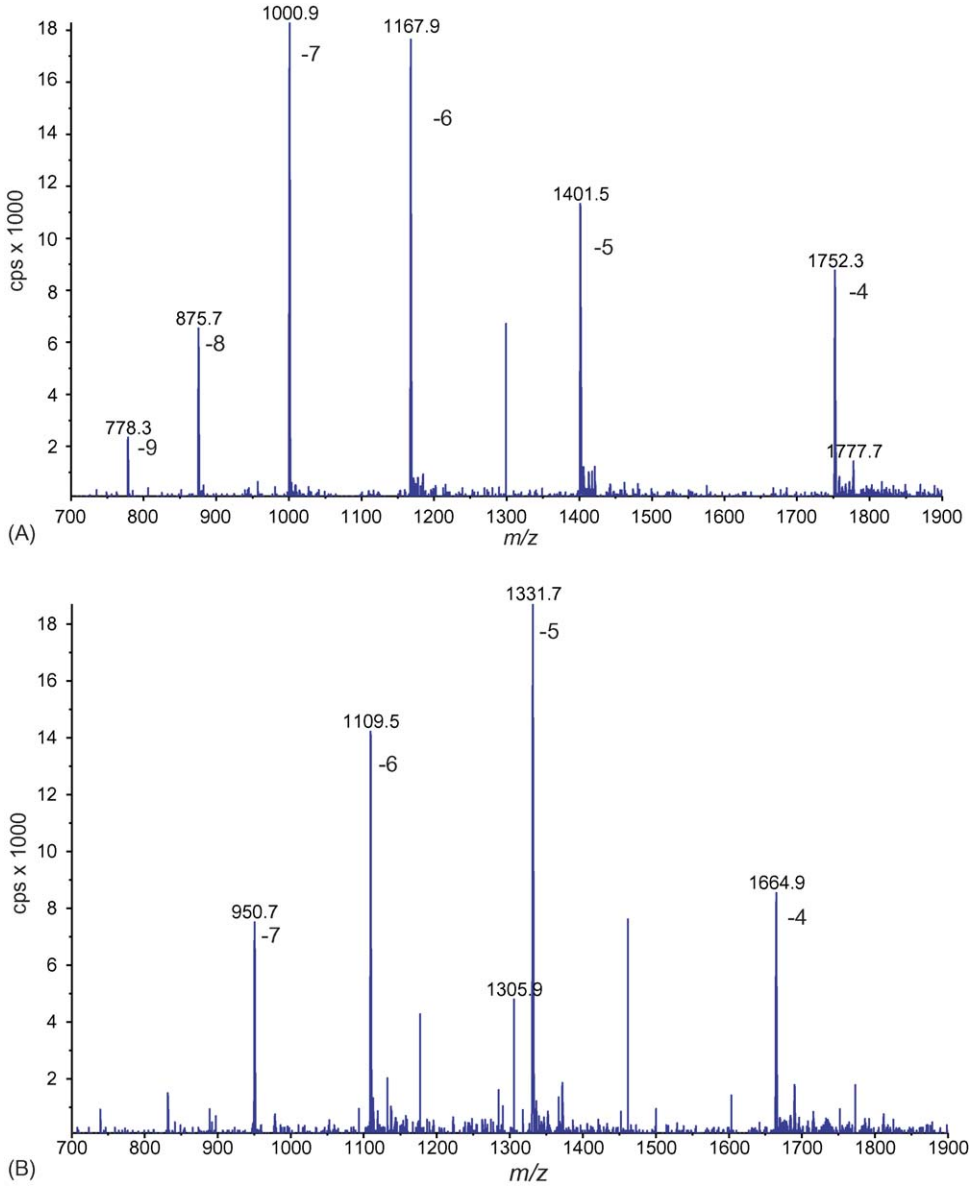

Fig. 3. Electrospray ionization spectra of (A) sense strand and (B) antisense strand showing the various charge states observed.

over the course of the experiment. This decrease is attributed to clearance of the oligonucleotide from the vitreous fluid.

3.2. Duplex analysis

The identified metabolites from the denatured single strands created a picture showing that the sense strand was degrading from the 5′ end and the antisense strand was degrading from the 3′ end. Since these strands are joined complementarily to form the duplex, these results inferred that the duplex was being preferentially degraded from one end.

Although examination of the oligonucleotides in their single strand form allowed identification of the metabolites, it did not provide direct information on how the degraded duplex existed. By denaturing the duplex there is no way to know how the individual single strand metabolites were originally paired or if any existed as single strands alone. Using different chromatographic conditions that did not denature the duplex, ESI was used to identify the intact duplex and to determine which metabolite species were paired to one another.

The chromatogram of a vitreous sample at Day 1 is shown in Fig. 5 along with its deconvoluted ESI mass spectrum. The peak shape of the duplex was broad but the ESI mass spectrum clearly showed the presence of the duplex and no metabolite species were detected anywhere in the peak. Again, it is important to note that the single strand species that appear in the mass spectra are caused by the ESI source and not the chromatography as the individual single strands eluted at different times than the duplex.

Metabolism of the duplex was easily observed in the chromatogram of the Day 4 vitreous sample (Fig. 6A). Compared to the Day 1 sample, the vitreous sample at Day 4 contained several peaks in its chromatogram however, the broad peak shape of the duplex prevented baseline separation. Despite the unresolved chromatogram, the mass spectra of distinct species were

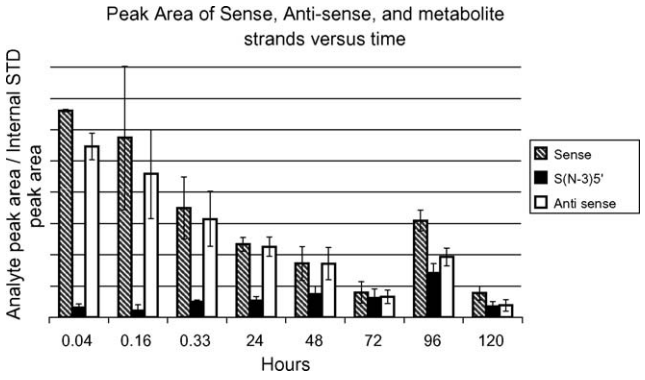

Fig. 4. Graph of the full-length sense, antisense and sense S(N-3)5′ metabolite peak areas from the UV 260 nm chromatograms over the various time points of the experiment. Analyte peak areas were normalized to the internal standard peak area. The values for time points 96 and 120 show increased values because 10× more of these samples were extracted than previous samples. Each time point shows the average ± S.D. ($n = 3$).

observed. The deconvoluted mass spectra for the peaks eluting between 14 and 16 min contained the mass of the full-length duplex as well as the masses of duplexes made up of various metabolites (Fig. 6B). The largest peak in the chromatogram of the 4-day time point at 14.9 min corresponded to a duplex composed of the S(N-3)5′/AS. The peak at 15.4 min corresponded to intact duplex; it is not clear why the elution time of the full-length duplex shifted from the Day 1 sample. The mass spectra from the less resolved early eluting peaks produced masses that corresponded to duplexes made up of various metabolite species such as one composed of the S(N-3)5′/AS(N-4)3.

All the identified duplex metabolites are listed in Table 2. The single strand components of these duplexes were also visible in the spectrum due to the denaturing caused by the ESI source (Fig. 6B). A benefit of the denaturing of the duplex by ESI is that the appearance of the single strand species can be used to confirm the identity of the duplex. While almost all of the duplex species detected were observed in the single stranded analyses, only a few of the many single stranded species were detected as duplexes. This is most likely a result of the lower sensitivity of the duplex analysis method. Mass spectra of intact duplex were much harder to obtain due to the extensive cation adduction and therefore, only the most abundant duplex species were observed. The detection of the intact duplex by MS was roughly 5–10 times less sensitive than the detection of the single stranded species.

A possible phenomenon that could give false information on duplex metabolites would be denaturing of the duplex, either on column or during the ESI process, followed by annealing of the single strands to form new duplexes not present originally. Such behaviour would give a false picture of how the duplex existed. In order to evaluate that there was no annealing of single strands to form new duplexes, a sample of the duplex was spiked with a synthesized S(N-3)5′ single strand metabolite at twice the concentration of the duplex and then analyzed. The resulting chromatogram contained a large peak representing the S(N-3)5′ single strand which eluted before the poorly resolved duplex (data not shown). The deconvoluted ESI spectrum of the duplex peak reported the mass of the full-length duplex and its single strand components. Importantly, the spectrum did not contain a mass corresponding to a duplex containing the N-3 metabolite

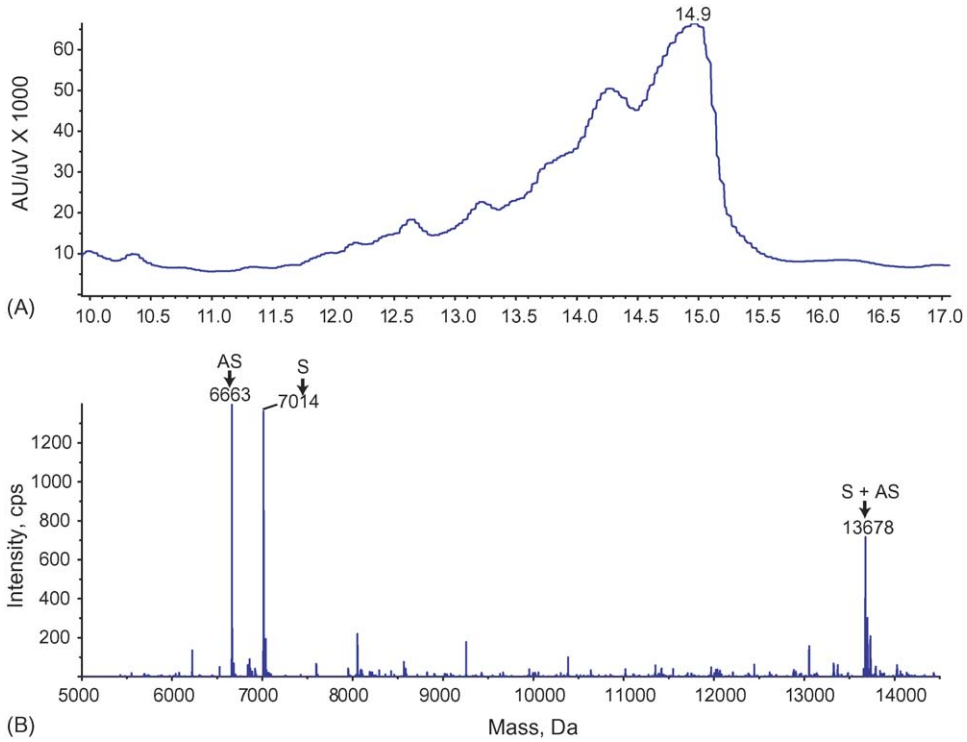

Fig. 5. (A) UV260 nm chromatogram of the Day 1 vitreous extract sample analyzed under non-denaturing reversed-phase conditions. (B) The deconvoluted ESI mass spectrum of the above chromatogram from 14 to 16 min. The intact duplex is observed at mass 13,678 as are the single strands at 7014 and 6663.

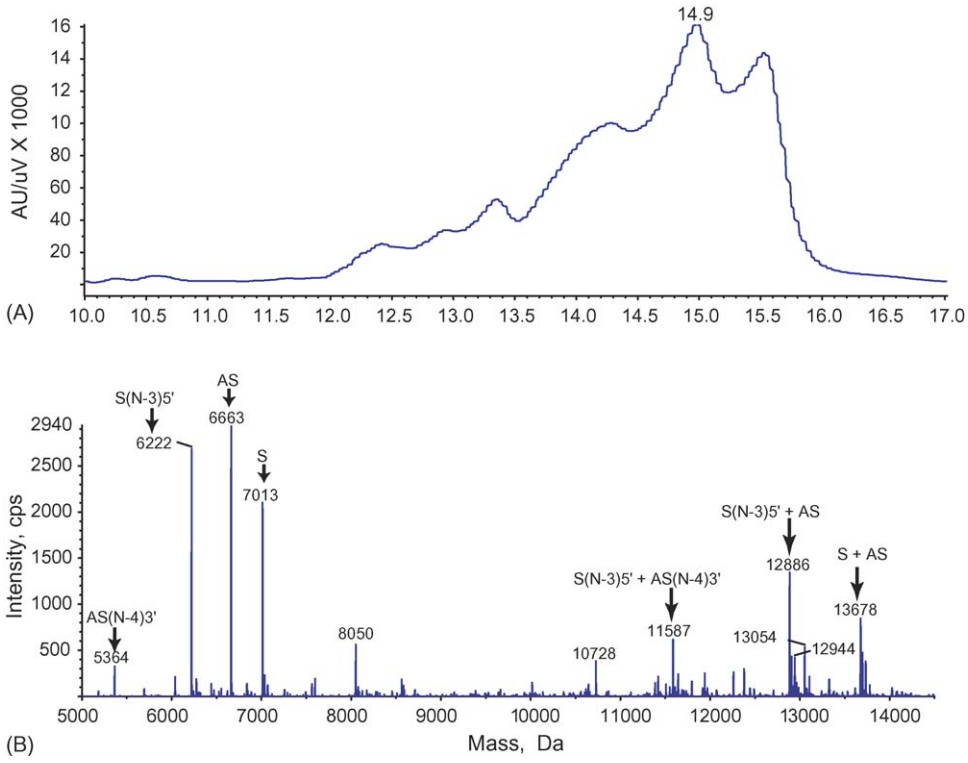

Fig. 6. (A) UV260 nm chromatogram of the Day 4 vitreous extract sample analyzed under non-denaturing reversed-phase conditions. (B) Mass spectra collected from 14 to 16 min in the UV chromatogram are deconvoluted and shown in the lower box. The full-length duplex is observed at mass 13,678 as are two duplexes made up of metabolites at 12,886 and 11,587. Also visible are the full-length single strands at 7013 and 6663 and two metabolite strands at 6222 and 5364.

Table 2
Duplex species observed from the non denaturing LC/MS analysis of vitreous samples

Duplex Metabolites	Nucleotide loss	Observed mass	Theoretical mass
5' BCUGAGUUUAAAAGGCACCCTTB	S	13678	13676.2
3' TsTGACUCAAAUUUUCCGUGGG	AS		
5' GAGUUUAAAAGGCACCCTTB	S(N-3)5'	12886	12884.7
3' TsTGACUCAAAUUUUCCGUGGG	AS		
5' GAGUUUAAAAGGCACCCTTB	S(N-3)5'	11587	11585.8
3' CUCAAAUUUUCCGUGGG	AS(N-4)3'		
5' AAAAGGCACCCTTB	S(N-9)5'	7823	7823.6
3' UUUUCCGUGGG	AS(N-10)3'		

indicating that mixing between the full-length and metabolite strands had not occurred.

4. Conclusion

Analysis of SIRNA-027 as single strands and as a duplex revealed a pattern of degradation demonstrating that the duplex was degrading primarily from one end; the degradation was on the 3′ end of the antisense strand and on the 5′ end of the sense strand. Nuclease preference to attack one particular site or side of the duplex could be due to the single strand nature of the duplex. If one end of the duplex were more easily relaxed into its single strands then that end could be more susceptible to degradation. Binding energy calculations done on the duplex revealed a difference of 2.5–3 kcal/mol in binding energy between the two ends of the SIRNA-027 duplex [38]. The degraded end of the duplex has the lower binding energy which, supports the idea that the ability of the duplex to relax into single strands plays a role in degradation. A duplex without the abasic and phosphorothioate groups showed a similar degradation profile although with not as clear a preference for one side of the duplex (some degradation of the 3′ end of the sense strand was observed) indicating that the chemical modifications also play a role in directing the degradation.

Acknowledgment

Thanks to Jim McSwiggen for supplying the Mfold binding energies for the duplex.

References

[1] A. Fire, S. Xu, M.K. Montgomery, S.A. Kostas, S.E. Driver, C.C. Mello, Nature (London) 391 (1998) 806.
[2] S.M. Elbashir, J. Harborth, W. Lendeckel, A. Yalcin, K. Weber, T. Tuschl, Nature (London) 411 (2001) 494.
[3] B.L. Bass, Cell (Cambridge, Mass) 101 (2000) 235.
[4] B.D. Lindenbach, C.M. Rice, Mol. Cell 9 (2002) 925.
[5] R. Agami, Curr. Opin. Chem. Biol. 6 (2002) 829.
[6] J.M. Silva, S.M. Hammond, G.J. Hannon, Trends Mol. Med. 8 (2002) 505.
[7] J.M. Alisky, B.L. Davidson, Am. J. PharmacoGenomics 4 (2004) 45.
[8] J.B. Berletch, J. Green, A.P. Cunningham, L.G. Andrews, T.O. Tollefsbol, Curr. Pharmacogenomics 2 (2004) 313.
[9] S. Barik, Ann. Med. (Basingstoke, United Kingdom) 36 (2004) 540.
[10] H. Gaus, S. Owens, M. Winniman, S. Cooper, L. Cummins, Anal. Chem. 69 (1997) 313.
[11] R. Griffey, M. Greig, H. Gaus, K. Liu, D. Monteith, M. Winniman, L. Cummins, J. Mass Spectrom. 32 (1997) 305.
[12] S.D. Rose, D.-H. Kim, M. Amarzguioui, J.D. Heidel, M.A. Collingwood, M.E. Davis, J.J. Rossi, M.A. Behlke, Nucleic Acids Res. 33 (2005) 4140.
[13] K. Light-Wahl, D. Springer, B. Winger, C. Edmonds, D. Camp, B. Thrall, R. Smith, J. Am. Chem. Soc. 115 (1993) 803.
[14] E. Bayer, T. Bauer, K. Schmeer, K. Bleicher, M. Maier, H. Gaus, Anal. Chem. 66 (1994) 3858.
[15] D.C. Gale, R.D. Smith, J. Am. Soc. Mass Spectrom. 6 (1995) 1154.
[16] J.A. Loo, Mass Spectrom. Rev. 16 (1997) 1.
[17] P.D. Schnier, J.S. Klassen, E.F. Strittmatter, E.R. Williams, J. Am. Chem. Soc. 120 (1998) 9605.
[18] V. Gabelica, E. De Pauw, J. Mass Spectrom. 36 (2001) 397.
[19] P. Rodrigues Hoyne, L. Benson, T. Veenstra, L.J. Maher, Rapid Commun. Mass Spectrom. 15 (2001) 1539.
[20] J. Beck, M. Colgrave, S. Ralph, M. Sheil, Mass Spectrom. Rev. 20 (2001) 61.
[21] J.B. Mangrum, J.W. Flora, D.C. Muddiman, J. Am. Soc. Mass Spectrom. 13 (2002) 232.
[22] M. Beverly, K. Hartsough, L. Machemer, Rapid Commun. Mass Spectrom. 19 (2005) 1675.
[23] A. Apffel, J. Chakel, S. Fischer, K. Lichtenwalter, W. Hancock, Anal. Chem. 69 (1997) 1320.
[24] A. Apffel, J. Chakel, S. Fischer, K. Lichtenwalter, W. Hancock, J. Chromatogr. A 777 (1997) 3.
[25] J.A. McCloskey, A.B. Whitehill, J. Rozenski, F. Qui, P.F. Crain, Nucleosides Nucleotides 18 (1999) 1549.
[26] A. Premstaller, H. Oberacher, C.G. Huber, Anal. Chem. 72 (2000) 4386.
[27] M. Gilar, Anal. Biochem. 298 (2001) 196.
[28] C.G. Huber, H. Oberacher, Mass Spectrom. Rev. 20 (2001) 310.
[29] K.J. Fountain, M. Gilar, J.C. Gebler, Rapid Commun. Mass Spectrom. 17 (2003) 646.
[30] C.G. Huber, A. Krajete, Anal. Chem. 71 (1999) 3730.
[31] H. Oberacher, W. Parson, S. Muhlmann, C.G. Huber, Anal. Chem. 73 (2001) 5109.
[32] J. Ambati, B.K. Ambati, S.H. Yoo, S. Lanchulev, A. Adamis, Surv. Opthalmol. 48 (2003) 257.
[33] F.E. Wincott, A. DiRenzo, C. Shaffer, S. Grimm, D. Tracz, C. Workman, D. Sweedler, C. Gonzalez, S. Scaringe, N. Usman, Nucleic Acids Res. 23 (1995) 2677.
[34] L. Beigelman, A. Karpeisky, N. Usman, Bioorg. Med. Chem. Lett. 4 (1994) 1715.
[35] L. Beigelman, J. McSwiggen, K. Draper, C. Gonzalez, K. Jensen, A. Karpeisky, A. Modak, J. Matulic-Adamic, A. DiRenzo, P. Haeberli, D. Sweedler, D. Tracz, S. Grimm, F. Wincott, V. Thackray, N. Usman, J. Biol. Chem. 270 (1995) 25702.
[36] F. Eckstein, G. Gish, Trends Biochem. Sci. 14 (1989) 97.
[37] D.A. Braasch, S. Jensen, Y. Liu, K. Kaur, K. Arar, M.A. White, D.R. Corey, Biochemistry (Mosc) 42 (2003) 7967.
[38] M. Zuker, D. Mathews, D. Turner, in: J. Barciszewski, B.F.C. Clark (Eds.), Algorithms and Thermodynamics for RNA Secondary Structure Prediction: A Practical Guide in RNA Biochemistry and Biotechnology, Kluwer Academic Publishers, 1999.